JOURNAL OF MATERIALS SCIENCE 22 (1987) 2899–2905

Internal fracture in an elastomer containing a rigid inclusion

K. CHO, A. N. GENT
Institute of Polymer Science, The University of Akron, Akron, Ohio 44325, USA
P. S. LAM
Research Division, The Goodyear Tire and Rubber Company, Akron, Ohio 44316, USA

Rubber blocks were prepared with thin glass rods in their centres, firmly bonded to the surrounding rubber. A tensile stress applied to the ends of a block in the direction of the rod axis induced the sudden formation of voids in the rubber near the flat ends of the rod. Approximate values of the local stresses have been calculated by FEM, assuming linear elastic behaviour. Voids were found to form when and where the local dilatant stress, $-P$ (negative hydrostatic pressure), exceeded the magnitude of Young's modulus, E, for the rubber. A precursor void in a highly elastic solid would expand indefinitely under these circumstances, so that fracture seems to be the result of an elastic instability. The applied stress at which voids appear was of the same order as E for short rods, or for a butt joint between a rod and a rubber cylinder of the same diameter, but it became extremely small when the rod was thin compared to the block in which it was embedded, and relatively long. Under these circumstances the local dilatant stress is calculated to be a large multiple of the applied tensile stress.

1. Introduction

Composites, consisting of high-modulus fibres or particles embedded in a softer matrix, are an important class of structural materials. However, the edges and surfaces of the inclusions can act as sites of dangerous stress concentrations and cause internal failure of the softer matrix material. Most previous work has dealt with the problem of stress transfer between the inclusion and the matrix [1–6]; few studies of matrix fracture induced by the inclusion have been reported [7–9].

One particular mode of fracture is considered here. Termed cavitation, it consists of the sudden appearance of a void within an elastomeric solid when the triaxial tension, $-P$ (negative hydrostatic pressure), at that point reaches a critical value, denoted P_c. This process is regarded as the unstable elastic expansion of a pre-existing void, too small to be readily detected, followed by its growth as a running crack when the maximum elongation of the material has been exceeded [7]. Growth of the void stops when it becomes large enough to alleviate the triaxial tension which gave rise to it.

In a previous study, cavitation was observed in an elastomeric matrix containing a rigid spherical inclusion [9]. Voids formed near the surface of the inclusion in the direction of the applied tension when the magnitude of the far-field tensile stress reached a critical value, t_c. For large inclusions, having a diameter, d, of 5 mm or more, the critical applied stress was found to be about $E/2$, where E is Young's modulus of the matrix elastomer. This corresponds to a triaxial tension at the poles of the inclusion of approximately E, in good agreement with the theoretical value for cavitation by the unbounded expansion of a precursor void in an incompressible highly elastic solid, i.e. $5E/6$ [7].

Larger stresses were found to be necessary to cause cavitation in the vicinity of smaller inclusions, although it is not at all clear why this is so. An empirical relation was found to hold [9]:

$$t_c = (5E/12) + k/d^{1/2}$$

where k is an experimentally determined constant, 25 to 40 kPa $m^{1/2}$.

We turn now to the phenomenon of cavitation near the flat end surfaces of a rigid rod, embedded in an elastomeric matrix which is subjected at infinity to a simple tensile stress in the direction of the rod axis. Two special cases are emphasized: the short rod, corresponding to a thin disc in the interior of the elastomeric material; and a rod that is long in comparison with the lateral dimensions of the sample containing it, so that it is effectively semi-infinite in length.

The general nature of the observed failures is described first and then some numerical values of the failure stresses are given and compared with theoretical estimates of cavitation stresses. In order to make these comparisons, values of the triaxial tension set up near the end surfaces of the rods have been computed using a finite-element method, assuming that the matrix material is linearly elastic and incompressible and that the inclusion is rigid and perfectly bonded to the matrix.

2. Experimental procedures

2.1. Preparation of test-pieces

Inclusions were prepared by cutting and polishing

0022–2461/87 $03.00 + .12

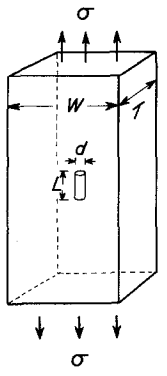

Figure 1 Rubber block, containing a glass rod at its centre, subjected to an applied tensile stress.

soda-lime glass rods of varied length and having diameters in the range 0.6 to 2.2 mm. Care was taken to ensure that the end surfaces were flat and that the edges were sharp. The rods were treated with a dilute solution of vinyltriethoxy silane in water, using acetic acid as a catalyst, to obtain good bonding later to the elastomeric matrix [10].

After dipping in the treatment solution, the rods were heated for 30 min at 110° C to promote reaction of the silane with the glass surface. They were then placed in the centre of a rectangular strip of natural rubber (SMR-5, Rubber Research Institute of Malaysia) containing 2% by weight of dicumyl peroxide. The composite specimen was placed in a heated press for 60 min at 150° C so that decomposition of the peroxide took place and the rubber became cross-linked, changing from a soft plastic material into a highly elastic solid. Simultaneously, a strong bond was formed with the glass inclusion.

The value of Young's modulus for the cross-linked rubber was found to be 1.5 MPa, much lower than that of glass, about 10 GPa. Thus, the rod-like inclusions can be treated as rigid in comparison with the rubber.

2.2. Measurement of critical stress

A sketch of a test specimen is shown in Fig. 1. The thickness, T, of the rubber block was generally chosen to be at least three times the diameter, d, of the centrally located rod and the width, W, was made generally about twice as large as T. Thus, the rod was effectively located within a thick rubber block. Nevertheless, the rubber was sufficiently transparent to permit visual inspection of the region around the rod ends with a low-power microscope.

This region was continuously monitored while the rubber was being stretched at a strain rate of about $4 \times 10^{-4}\,\text{sec}^{-1}$ (measured on that portion of the sample that did not contain the inclusion). Some typical observations are described in the following section. A measurement of the tensile strain, e, in the part of the sample away from the inclusion was made at the moment when the first void suddenly appeared at the rod end. This measurement was made by means of an ink grid applied to the rubber surface in the unstrained state. The critical strain level was then converted into a corresponding critical value of the applied stress, t, from the previously determined relation between tensile stress and extension for the rubber.

3. Experimental results and discussion

3.1. Qualitative observations

The development of internal fractures is shown in Fig. 2 for a specimen containing a short glass rod, $L/d = 1$. When the far-field tensile strain reached a critical value of about 100% a small cavity appeared close to one flat end of the rod and close to the rod edge. Then at a somewhat higher strain level a second cavity appeared near the centre of the flat surface of the rod and another cavity appeared at the other end of the rod, again near the edge. On stretching further, other cavities appeared and linked up, at least partially, to form large pointed voids at both ends of the rod (Fig. 2).

Quite similar processes were observed with a long glass rod, $L/d = 5$ (Fig. 3), although the critical value of the far-field tensile strain was somewhat smaller in this case, about 60%. It is again noteworthy that the first cavities appeared toward the edges of the flat end surfaces, followed by cavities in the central region at somewhat higher strain levels.

3.2. Proposed mechanism of failure

A proposed sequence of failure events corresponding to the observed development of voids is shown in Fig. 4. At first, a hypothetical precursor void, too

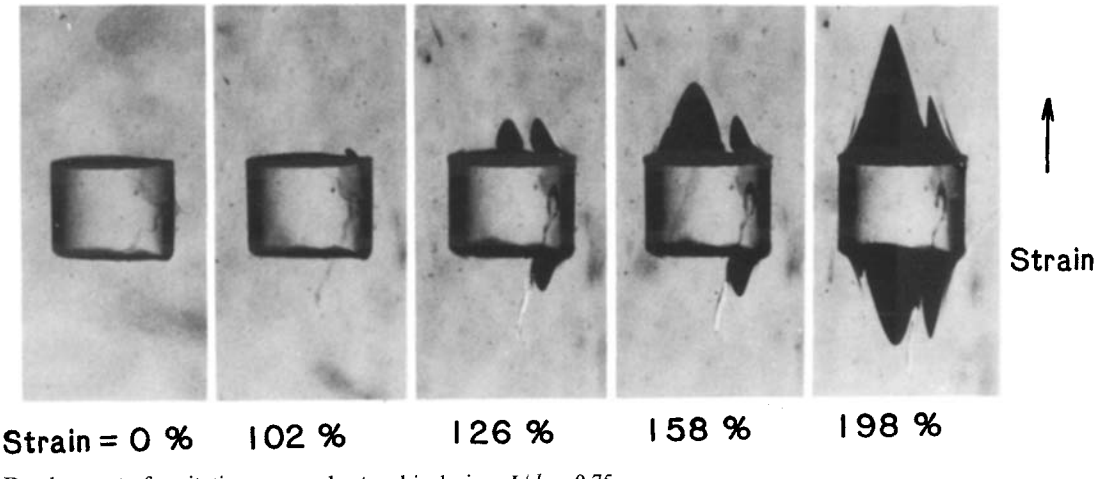

Figure 2 Development of cavitation near a short rod inclusion, $L/d = 0.75$.

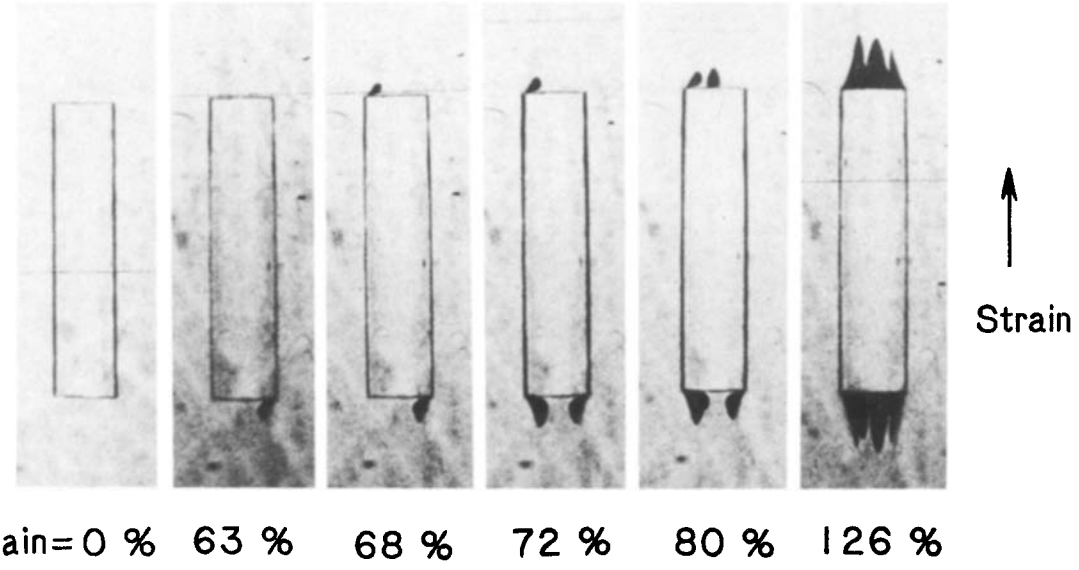

Figure 3 Development of cavitation near a long rod inclusion, $L/d = 5$.

small to see, expands under the large triaxial tension, $-P$, acting near the flat surface of the rod (Fig. 4a). When the degree of expansion exceeds the maximum extensibility of the rubber, the void wall will split apart and the cavity will grow further by tearing (Figs 4b, c) to reach a visible size. At somewhat higher stresses, other voids, situated in less favourable locations or of smaller size, will also be induced to grow into large. visible cavities (Fig. 4d). However, they are still at this stage entirely surrounded by rubber. Although they are formed close to the surface of the inclusion, where the dilatant stress is largest, they do not make contact with the rigid surface. They can be distinguished from voids formed by detachment from weakly bonded inclusions by the characteristic "convex lens" shape of the regions between the void and the surface of the inclusion. Indeed, it is sometimes possible to see the thin layer of rubber remaining between the void and the inclusion. However, at still larger stresses the shape of that part of the void in close proximity to the inclusion surface undergoes a marked change (Fig. 4e), which is attributed to detachment from the inclusion and rupture of the layer of rubber separating the void from it. Finally, the cavities link up by further detachment and tearing apart of the layers of rubber separating them (Fig. 4f). These several stages can be recognised in Figs 2 and 3.

It is noteworthy that the voids do not lead directly to fracture of the specimen. Because they are oriented in the direction of the applied stress they can grow to a substantial size without becoming unstable.

3.3. Cavitation stresses

We now turn to the critical conditions for formation of the first visible voids. Values of the applied stress, t_c, at which the first void appeared near the rod end are plotted in Fig. 5 against the length, L, of the rod for two different widths, W, of the rubber block. The rod diameter, d, was relatively small in comparison with the width or thickness of the rubber block so that when the rod length, L, was also small it became a small thin disc located in the centre of a large rubber block with its axis parallel to the direction of the applied tension. Under these circumstances the critical

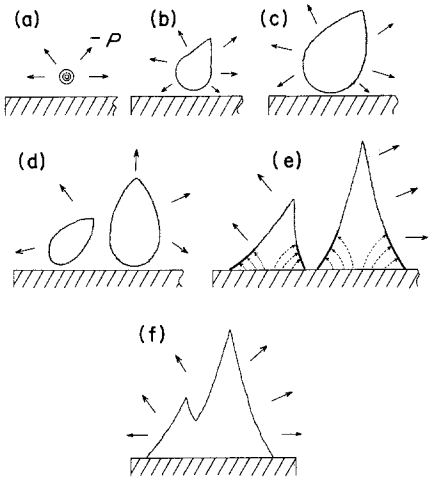

Figure 4 Sketch of proposed development of internal failures from hypothetical precursor voids. (a) Elastic expansion of a precursor void, (b, c) growth by tearing to a visible size, (d) multiple cavities, (e) detachment from the substrate, (f) joining up by detachment or tearing.

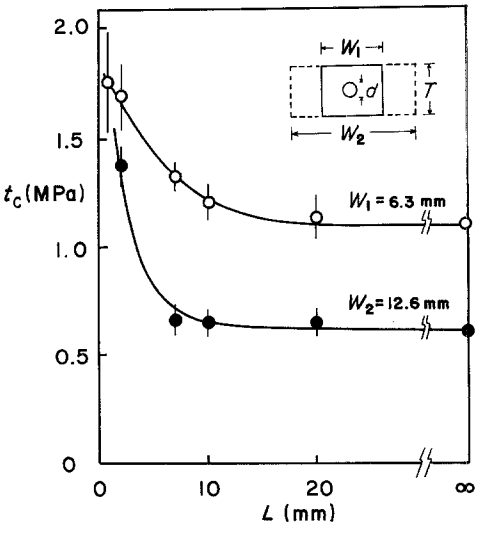

Figure 5 Effect of length, L, of rod on the critical applied stress for cavitation for two different widths, W, of rubber block. Block thickness, T, 4.8 mm. Rod diameter, d, 2.2 mm.

applied stress for cavitation was found to be about 1.75 MPa, and independent of the width or thickness of the rubber block.

When the rod was longer, however, the critical stress was appreciably lower and it now depended upon the width and thickness of the rubber block (Fig. 5). When the block had a large cross-section, the critical stress for void formation at the end of a long rod was small, and vice versa.

The two extreme cases (a short rod or a small disc in the centre of a thick rubber block, and a long rod embedded in a block of varied width and thickness) are now considered separately.

3.4. Short rod or disc inclusions

Values of the critical applied stress were determined for short-rod inclusions ($L/d \simeq 1$) and for small glass cubes arranged so that two of the faces were normal to the far-field tensile stress. The results were virtually identical and independent of the length or diameter over the range investigated, 0.6 to 2.2 mm, as shown in Fig. 6. The mean value of the true far-field cavitation stress, t_c (given by $(1 + e)\sigma_c$ where σ_c is the engineering critical stress, i.e. the applied force per unit of undeformed cross-sectional area), was 1.42 MPa.

From finite-element calculations, described in the Appendix, the dilatant stress, $-P$, acting in the surface plane of a thin rigid disc, located at the centre of a thick block of an incompressible linearly elastic material was found to be substantially uniform over the surface of the disc, out to a radius $r = 0.85(d/2)$ and approximately equal to the applied far-field tensile stress (Fig. 7). Thus, the criterion for formation of the first cavity appears to be that the local dilatant stress, 1.42 MPa in the present case, reaches a value of the same order as Young's modulus, E, for the elastomer; 1.5 MPa for the natural rubber compound employed here. This is in good agreement with the critical condition for the unbounded elastic expansion of a small spherical cavity in a block of highly elastic solid [7].

It is interesting to compare cavitation near the flat surface of a disc or cube with the corresponding process near a rigid spherical inclusion. Results for spherical inclusions of various diameters, taken from

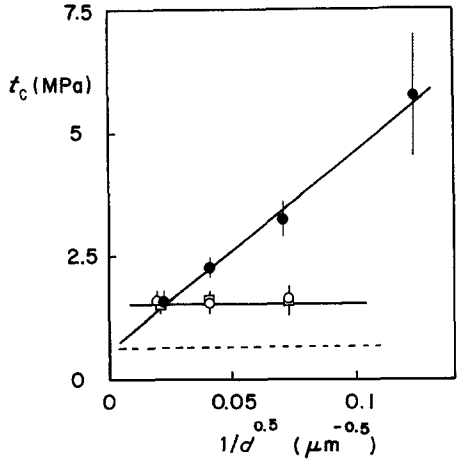

Figure 6 Critical stresses for cavitation near (○) a short rod or (□) cube inclusion and (●) near a spherical inclusion [9] plotted against diameter or width, d, of inclusion.

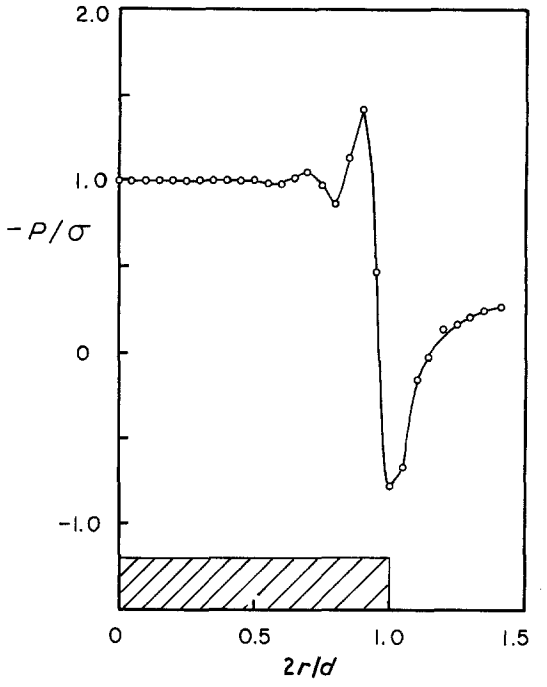

Figure 7 Computed distribution of dilatant stress $-P$ near the surface of a thin rigid disc with its axis in the direction of the applied far-field tensile stress, σ.

an earlier investigation [9], are shown in Fig. 6 for comparison. The critical stresses for spherical inclusions depended strongly upon the size of the inclusion. They were only in good accord with the theoretical prediction $-P \simeq E$, corresponding to $\sigma_c \simeq E/2$ for a spherical inclusion, when the diameter, d, was relatively large, several mm or greater. For smaller diameters, about 1 mm or so, the critical stress was about twice as large as predicted and it increased sharply as the diameter of the inclusion was reduced further (Fig. 6).

This anomalous behaviour might reflect the relatively small volume of material at the poles of a spherical inclusion that is subjected to a large dilatant stress, in comparison to that near the flat surface of a disc of similar diameter. If precursor voids of sufficient size to become elastically unstable when $-P \simeq E$ are distributed sparsely, so that there are few or none in a volume of less than, say, 10^{-14} m^3, then higher stresses would be needed to induce cavitation when the volume under a dilatant stress is as small as this. For a spherical inclusion having a diameter of 1 mm, the volume under a large dilatant stress is only of this order of magnitude. For a disc of the same diameter, the corresponding volume of rubber under a high dilatant stress is about 10^{-10} m^3, several orders of magnitude larger, and precursor voids of sufficient size may then be plentiful.

Experiments with discs of much smaller diameter would be helpful to examine whether the critical stress for cavitation is then larger than predicted, in the same way that it is for spherical inclusions of about 1 mm diameter.

3.5. Long rod inclusions

The experimental method used for studying cavitation near the flat end surface of a rod of semi-infinite length is shown in Fig. 8. Wide ranges of width and thickness of the rubber block were employed. At one extreme,

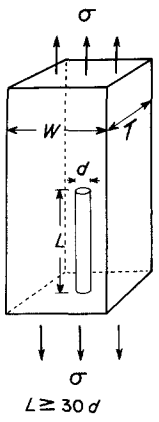

Figure 8 Sketch of experimental arrangement for a rod of semi-infinite length.

the block had the same cross-section as the glass rod and was joined to it end-to-end as a butt joint. In this case, $W = d$. The other extreme case employed a rubber block having a width and thickness of about $10d$. Two different diameters of glass rod were used, about 0.6 and about 2.2 mm.

Measured values of the applied stress at which a cavity first appeared are plotted in Fig. 9 against the ratio d/W of the rod diameter to the width and thickness of the square-sided block. Results are given for cavities which first appeared near the edge of the rod end surface, open points, and for cavities appearing near the centre, filled-in points. Cavities at the edge generally formed first, at somewhat lower stresses.

The critical stresses were found to be independent of the diameter, d, of the rod, over the limited range studied, but they depended strongly upon the ratio d/W. For the butt-joined test-piece, when $d/W = 1$, the true applied stress was about 5 MPa and the engineering applied stress was about 1.5 MPa for cavitation. At the other extreme, cavities formed at an applied stress of only about 0.3 MPa when the rod diameter was much smaller than the width and thickness of the rubber block (Fig. 9).

Before discussing theoretical estimates of the cavitation stress, represented by the broken curves in Fig. 9, it should be explained why, in this figure, the results are given in terms of engineering stress instead of true stress. When the inclusion is small in comparison to the block in which it is embedded, the appropriate measure of far-field fracture stress is probably the true stress, as has been employed hitherto. In the present case, however, the long rod inclusion prevents the rubber surrounding it from undergoing a significant amount of extension and thus, almost up to the rod end, the rubber block retains its original cross-section. In the rest of the rubber block, on the other hand, the rubber stretches considerably and its cross-sectional area decreases correspondingly. Because Poissonian contraction is inhibited at the rod end to a marked degree, the relevant "far-field" stress seems to be that calculated on the basis of the original cross-sectional area, i.e. the engineering stress, σ, rather than the true stress, t, acting in that portion of the specimen that undergoes an unrestricted contraction in the cross-sectional area.

Using the finite-element method described in the Appendix, values of dilatant stress, $-P$ were computed as a function of radial distance, r, for a plane in a cylindrical elastic block lying close to the flat end of a long embedded rigid rod. Again, the block was assumed to be incompressible and linearly elastic. Results are shown in Fig. 10 for a block having a diameter, D, twice as large as that of the embedded rod, for planes at various distances, z, away from the flat end of the rod. When z is large, the dilatant stress is relatively uniform and given by $\sigma/3$ where σ is the applied far-field stress. When z is small, the dilatant stress is considerably larger and rises from a value of about 1.4σ at the centre of the rod end surface to a value of about 2σ near the edge. Because of possible

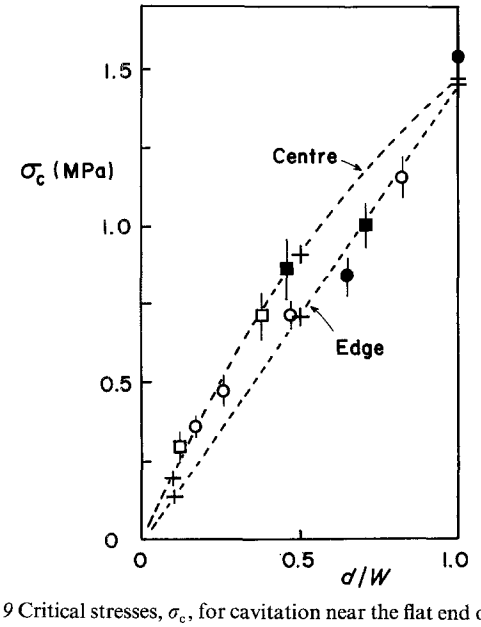

Figure 9 Critical stresses, σ_c, for cavitation near the flat end of a rod of semi-infinite length plotted against the ratio d/W of rod diameter, d, to width, W, of the rubber block in which it is embedded. (□, ■) rod diameter $d = 0.6$ mm; (○, ●) $d = 2.2$ mm. Crosses and broken curves, results obtained from FEM calculations, (Figs 10 and 11) assuming that $-P_c = 0.75E$.

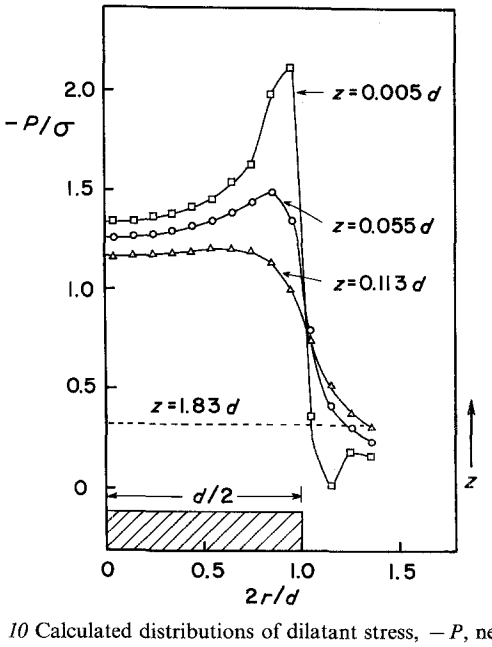

Figure 10 Calculated distributions of dilatant stress, $-P$, near the flat end of a long rigid rod of diameter, d, embedded in an elastic block of diameter $D = 2d$. The distance above the rod end is denoted by z. The far-field tensile stress is denoted by σ.

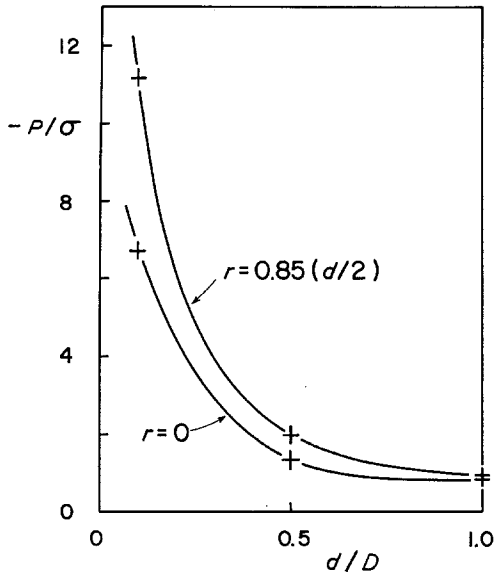

Figure 11 Calculated values of dilatant stress, $-P$ near the flat end of an embedded rod plotted against the ratio of the rod diameter, d, to the diameter, D, of the rubber block in which it is embedded. The far-field tensile stress is denoted by σ. Upper curve, $-P$ calculated at $r = 0.85(d/2)$; lower curve, $-P$ calculated at $r = 0$.

inaccuracy arising at the rod edge from stress singularities and the relatively coarse mesh used in these computations, with only 10 elements used for the rod radius, $d/2$, the dilatant stress in the vicinity of the rod edge has been taken at the radial distance, $r = 0.85(d/2)$, rather than at the singular edge point, $r = d/2$. These results, together with those obtained at the centre of the rod end surface, $r = 0$, are plotted in Fig. 11 against the ratio of the rod diameter, d, to the diameter, D, of the elastic block in which it is embedded.

When the rod diameter is equal to that of the block, corresponding to a butt joint between a rigid rod and an elastic one, the results show that the dilatant stress set up at the interface is approximately the same as the applied far-field tensile stress, except very near the edge where stress singularities dominate. When the rod is much smaller than the block in which it is embedded, the dilatant stress at the rod end is much larger than the far-field tensile stress and even larger towards the edge of the rod end surface.

These results can be employed to calculate theoretical values for the applied stress at which cavitation takes place, on the assumption that the critical condition for cavitation is that the dilatant stress approaches the magnitude of Young's modulus $-P \simeq E$. The broken curves in Fig. 9 were obtained in this way from the relations given in Fig. 11. They describe the experimentally measured conditions for cavity formation with considerable success, over the whole range of block dimensions. We conclude that dilatant stresses near the rod ends are, indeed, responsible for the observed failures, which take place when and where the dilatant stress approaches E in magnitude.

4. Conclusions

1. A characteristic internal fracture process, termed cavitation, is observed in a stretched elastomeric block containing a rigid disc or rod.

2. The critical applied stress at which cavities form is affected by the width and thickness of the rubber block and by the length of the rod. For a short rod, i.e. a disc, it is independent of the rod diameter and of the size of the rubber block in which it is embedded, and is approximately equal to Young's modulus, E, of the elastomer. For long rods, it is inversely proportional to the width and thickness of the rubber block and becomes quite small, less than $E/5$ when the width and thickness are ten times the rod diameter.

3. The first cavities form near the edges of the flat end surfaces of the rod. At higher stresses cavities also appear in the centre, but still close to the interface.

4. Stress distributions near the rod surface have been calculated by finite element methods, assuming perfect bonding of an incompressible, linearly elastic material.

5. The observed cavitation stresses are in satisfactory agreement in all cases with a simple fracture criterion: that voids form where, and when, the local dilatant stress $-P = E$. This is the same criterion that governs the unstable elastic expansion of a spherical void in a highly elastic solid and suggests that invisibly small precursor voids are plentiful in elastomeric solids.

Appendix. Finite element analysis

Stress distributions within the rubber block were analysed using a finite element method. The rubber block was treated as a long cylinder containing a long rigid rod or a thin rigid disc. The rod extended from one end of the rubber cylinder to its middle section. The length of rod was chosen to be thirty times its radius and the radius of the rubber cylinder was chosen to be one, two, or ten times the radius of the rod. In the case of the embedded disc, the radius of the rubber cylinder was taken to be ten times the radius of the disc, which was given a thickness (length) of zero. A uniform tensile stress was assumed to be applied at both ends of the rubber cylinder, of magnitude $E/100$, where E is Young's modulus of the rubber. The rubber was assumed to be linearly elastic and incompressible, with Poisson's ratio equal to 0.5. The rod and disc were assumed to be perfectly rigid.

The finite element model was analysed using the MARC program [11]. The incompressible restraint was enforced by the Herrmann variational principle [12] which treats the hydrostatic pressure as an independent variable.

The rubber matrix in the vicinity of the end of the rigid rod was mainly considered in the analysis, because fracture occurs in this region. Large stress gradients were expected; therefore, eight-noded quadrilateral axisymmetric elements with nine Gaussian integration points were used. There were ten equally spaced elements in the radius direction, along the interface, with an element height of $0.01d$ where d is the rod diameter. The element height was increased gradually for element layers lying further away from the interface.

Perfect bonding was assumed to exist between the rigid rod and the matrix. Hence, the boundary conditions at the interface were set up to disallow relative displacements between adjacent faces of the rigid

rod and the matrix. The computer program calculated stresses in the axial, radial and hoop directions; σ_{zz}, σ_{rr}, $\sigma_{\theta\theta}$. The dilatant stress, $-P = (\sigma_{zz} + \sigma_{rr} + \sigma_{\theta\theta})/3$, was evaluated at the centre of each element.

Acknowledgements

K. Cho and A. N. Gent acknowledge support of their research by a grant from the Office of Naval Research (Contract N00014-85-K-0222) and a grant-in-aid from Lord Corporation.

References

1. H. L. COX, *Brit. J. Appl. Phys.* **3** (1952) 72.
2. N. F. DOW, General Electric Co., Schenectady, New York, Report R635D 61 (1963).
3. D. M. SCHUSTER and E. SCALA, *Trans. Metal. Soc.* **230** (1964) 1635.
4. W. R. TYSON and G. W. DAVIES, *Brit. J. Appl. Phys.* **16** (1965) 199.
5. I. M. ALLISON and L. C. HOLLOWAY, *ibid.* **18** (1967) 979.
6. A. S. CARRARA and F. J. McGARRY, *J. Compos. Mater.* **2** (1968) 222.
7. A. N. GENT and P. B. LINDLEY, *Proc. R. Soc. (London)* **A249** (1959) 195.
8. A. E. OBERTH and R. S. BRUENNER, *Trans. Soc. Rheol.* **9** (1965) 165.
9. A. N. GENT and B. PARK, *J. Mater. Sci.* **19** (1984) 1947.
10. A. AHAGON and A. N. GENT, *J. Polym. Sci. Polym. Phys. Edn* **13** (1975) 1285.
11. MARC Analysis Research Corporation, Palo Alto, California, USA.
12. L. R. HERMANN, *AIAA* **3** (1965) 1896.

Received 29 September
and accepted 15 December 1986